ACS APPLIED ENGINEERING MATERIALS

pubs.acs.org/acsaenm Article

Electrospun Membranes Modified with Lanmodulin-Derived Peptides for Lanthanide Adsorption

Lianna Johnson,[§] Bernadette L. Schneider,[§] Husain Mithaiwala, Matthew D. Green, Julie N. Renner,* and Christine E. Duval*

Cite This: *ACS Appl. Eng. Mater.* 2024, 2, 2442−2453 Read Online

ACCESS | Metrics & More | Article Recommendations | Supporting Information

ABSTRACT: Rare earth elements (REEs) are crucial for clean energy technologies but are predominantly purified by solvent extraction using strong acids. This work explores two adsorbents with selective chemistry based on lanmodulin-derived peptides. Two membrane adsorber platforms were synthesized: (1) a poly(vinylbenzyl chloride) membrane with a grafted poly(allyl methacrylate) network and (2) a poly(arylene ether sulfone) membrane with allyl pendant groups. Both membrane adsorbers were functionalized with LanM1 peptides via a thiol−ene click reaction. The morphology, surface chemistry, and adsorption of select trivalent lanthanides (La, Ce, Pr, Nd) were characterized in pH 4−5 solutions, mimicking phosphogypsum waste streams. Results from the adsorption experiments indicate that the lanmodulin peptide sequence maintains its ability to bind when it is immobilized on the surface of polymer fibers for some ions. Despite the different adsorbent designs, the measured capacity of both adsorbents is on the same order of magnitude, which may be explained by differences in the surface area of the fibers.

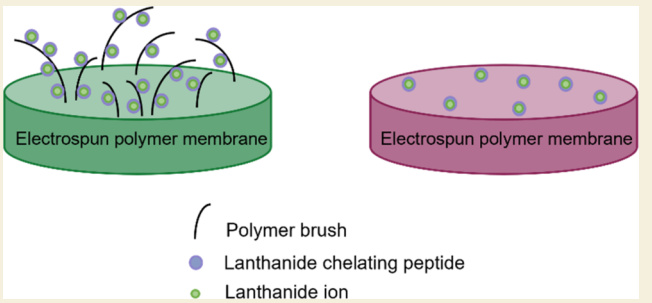

KEYWORDS: *rare earth elements, adsorption, affinity peptide, lanmodulin, biosorption*

1. INTRODUCTION

Rare earth elements (REEs) are crucial for modern technology, such as smartphones and clean energy. Currently, REEs are sourced from mined ore and then separated via solvent extraction.[1] Solvent extraction has several drawbacks as it requires hundreds of stages, produces mixed organic radioactive waste, and leaves a CO_2 footprint of approximately 55 kg CO_2 per kg lanthanide.[2] Industrial waste has been discovered as a potential source of REEs. For example, phosphogypsum, a radioactive byproduct of fertilizer production, contains an average of 0.1−0.2 wt % REEs[3,4] and has inspired global research on REE recovery from this waste stream.[3,5] Much of the phophogypsum is stored in open stacks, with an estimated 1 billion tons stored in the US state of Florida alone.[6] Recovering REEs from this waste could enable a significant contribution to the domestic consumption of REEs, which has been estimated at 9 kt annually.[7] Other potential REE sources are recycled nickel−metal hydride batteries and end-of-life electronic wastes.[8,9] For all feedstocks, REE recovery requires a two-step process including (1) concentrating the REEs and (2) separating them from each other in acidic solutions.

Adsorbent materials with selective ligands have been explored as a more sustainable alternative to solvent extraction. A commonly used adsorbent technology in small-scale REE separations is diglycolamide resins in chromatography columns. These functionalized resin beads have shown selectivities of 1.5−3 for neighboring lanthanides.[10] These selectivity values are generally low and are achieved only at high acid concentrations (pH 2 or lower). An emerging class of separation materials, biosorbents, have shown promising capability to separate ions selectively at more neutral pH—expanding conditions at which selective REE separations can be performed.[11,12] These materials are often resins or nanoparticles functionalized with REE-selective proteins or peptides.[13−17]

Membrane adsorbers are a separation technology that has advantages over resins like fast separation times[18] and minimal solvent use.[19] The drawback to using membrane adsorbers is they tend to have a lower binding capacity than their resin-based counterparts[19] due to lower surface areas. In related fields, this limitation has been overcome by grafting ligand-bearing polymer brush-like structures from the surface and pores of membranes, which increases the ligand density per surface area.[20] Previous work in our laboratory developed our first lanthanide-binding membrane materials. A poly(glycidyl

Received: August 9, 2024
Revised: September 27, 2024
Accepted: September 30, 2024
Published: October 7, 2024

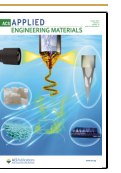

https://doi.org/10.1021/acsaenm.4c00510
ACS Appl. Eng. Mater. 2024, 2, 2442−2453

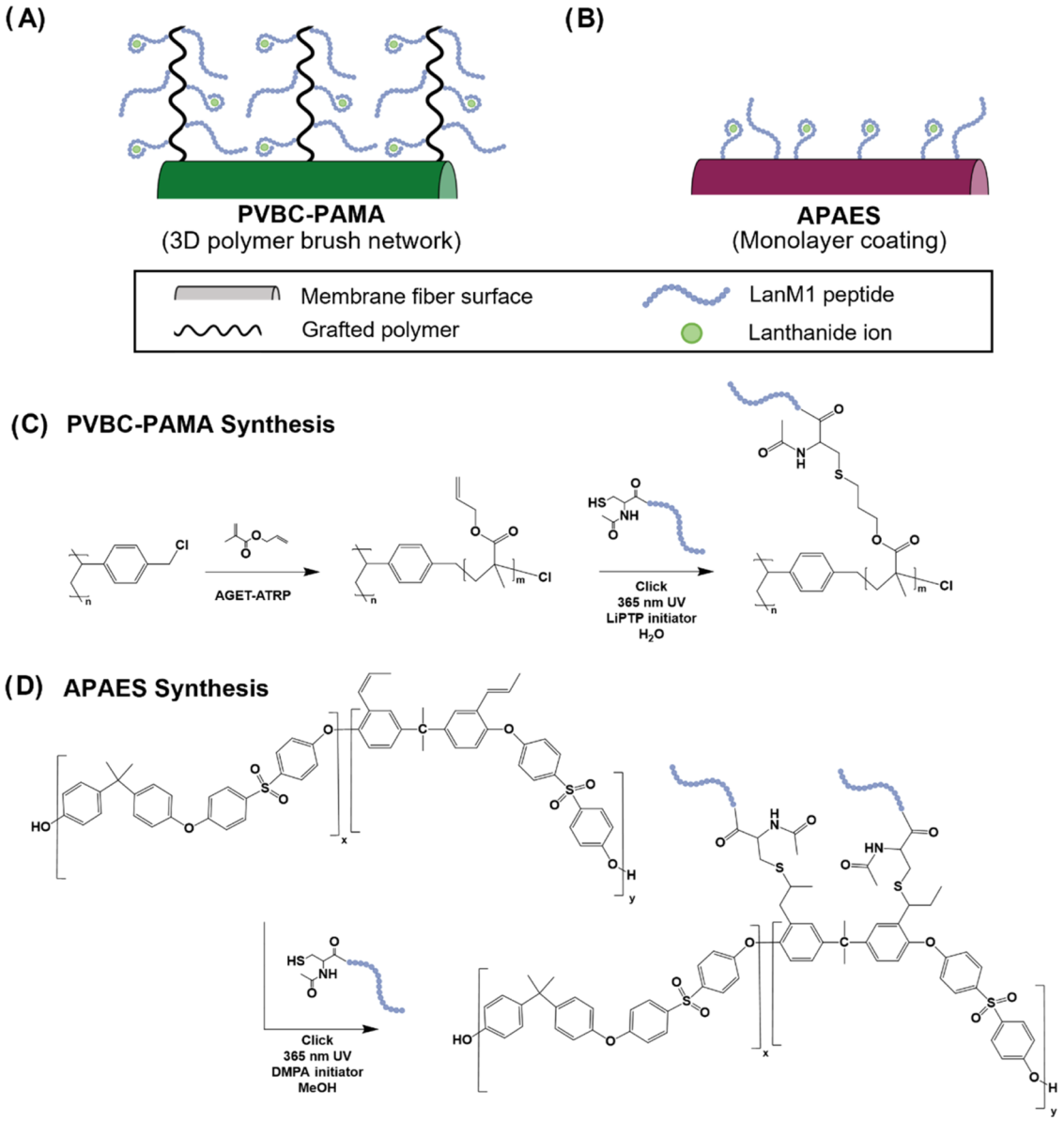

Figure 1. Visual representation of two peptide-functionalized membrane designs for lanthanide adsorption. (A) PVBC−PAMA, which has adsorption sites throughout a three-dimensional network of brush-like extensions grafted from the base fibers and (B) APAES which has a monolayer of peptide adsorption sites on the fibers. Synthetic schemes for the fabrication of (C) peptide-functionalized PVBC−PAMA membranes and (D) APAES membranes. Note: the alkene groups of the unreacted APAES polymer are represented as *cis* and *trans* isomers. In addition, the unsaturated group may be present as an isomerized terminal alkene.

methacrylate) polymer network was grafted from a commercial poly(ether sulfone) membrane via ultraviolet (UV)-initiated free radical polymerization.[21] The epoxide rings were subsequently reacted with lysine, which served as a ligand. Equilibrium adsorption experiments revealed good selectivity for light lanthanides over mono- and divalent metals, but selectivity between lanthanides remained low.

Biologically derived ligands are highly tunable and may serve as a platform for studying and designing new ligands that exhibit high ion−ion selectivity—as required for REE separations. Lanthanide-binding tag (LBT) peptides based on the metal-binding sequences known as EF-hands (natively found in calcium-binding proteins) have been explored for lanthanide biosorption.[22,23] Meanwhile, lanmodulin (LanM) proteins[24,25] have also captured researchers' interest in REE recovery from industrial waste. LanM proteins not only have high affinity (K_d ∼ pM) for REEs, but also a remarkable tolerance for acidic conditions (near pH 2.5) and high selectivity in the presence of competitor ions at 1000 fold excess.[26] Recent work targeting REE recovery and separation has used covalently attached lanthanide-binding peptides and LanM proteins on adsorptive resins,[13−15] on magnetic nanoparticles[16] as well as in elastin-based biomaterials to isolate lanthanides via induced phase transition.[27]

Using peptides instead of the full LanM protein for REE recovery has the potential advantage of higher packing of ligands on the solid support due to the smaller size of the biomolecule. When the LanM protein was bound to the resin, the stoichiometry of binding was found to be ∼2 Ln(III) ions per LanM protein. In contrast, the LanM protein in solution has three sites with high affinity and a fourth with weaker affinity, indicating that one of the high-affinity sites is

https://doi.org/10.1021/acsaenm.4c00510
ACS Appl. Eng. Mater. 2024, 2, 2442−2453

deactivated upon immobilization.[13] When isolated from the scaffold of the protein, the four metal-binding peptides from LanM have similar affinity with K_ds on the order of μM.[28] Previously, we found that when bound to a gold surface, an REE-binding peptide derived from calmodulin and a peptide from lanmodulin maintained or increased in affinity for REEs. The K_d estimates for Ce(III) are: calmodulin peptide, 1.3 μM on surface vs 2.9 μM in solution; LanM1, 0.9 μM on surface vs 3.8 μM in solution).[17,29] In a follow-up study, the calmodulin peptide was installed on a grafted polymer network and demonstrated that the calmodulin peptide maintained the ability to bind to cerium ions when covalently bound to a polymer scaffold.[30] In that approach, poly(glycidyl methacrylate) was grafted from a poly(vinylidene difluoride) (PVDF) membrane using activator generated electron transfer atom transfer radical polymerization (AGET-ATRP) and then the epoxide rings were converted to azide functional groups to enable a click cycloaddition reaction with an alkyne-terminated EF-hand loop peptide. While this initial study was an important proof-of-concept, confocal microscopy revealed that the functional coating was localized to the top surface of the membrane, ultimately limiting the capacity. One strategy to overcome this limitation is to employ membranes formed from polymers that incorporate AGET-ATRP initiators or click-chemistry moieties throughout the polymer backbone.[31] To date, an underexplored aspect of the bioadsorbent design and manufacturing is how the architecture of the surface impacts peptide−ion affinity and membrane capacity. Since the peptide has an entropy-driven binding mechanism[17] where folding of the peptide around the ion is thought to be important, we hypothesized that the membrane morphology may impact the peptide-lanthanide binding.

In this work, we tested this hypothesis by synthesizing two peptide-functionalized membrane platforms and conducting initial equilibrium adsorption studies. The first membrane platform is synthesized by (1) electrospinning poly(vinylbenzyl chloride) (PVBC) membranes, (2) cross-linking the PVBC membranes for chemical stability, (3) grafting poly(allyl methacrylate) (PAMA) via AGET-ATRP, and then (4) attaching the LanM1 peptide functionality via a thiol−ene click reaction. This synthesis scheme results in the structure shown in Figure 1A,C. The second membrane platform uses a specialty polymer with allyl pendant functional groups incorporated onto 50% of the monomer units of a poly(arylene ether sulfone) backbone i.e., allyl-modified poly(arylene ether sulfone) copolymers [PAES(50)-*co*-APAES(50)] referred to as APAES.[31−33] Membranes were fabricated by (1) electrospinning the APAES polymer and then (2) attaching LanM1 peptides via a thiol−ene click reaction directly onto the polymer backbone, according to the process shown in Figure 1B,D. Herein, membrane synthesis and functionalization with LanM1 peptides is described and membrane surface chemistry and morphology are analyzed. Membrane adsorption of select trivalent lanthanides (La, Ce, Pr, and Nd) was evaluated using equilibrium experiments for both membrane platforms at acidic pH (pH 4−5), which maintains solubility of REEs and mimics the pH of phosphogypsum remediation streams. This contribution is an important step toward using peptide-functionalized membrane adsorbers for REE purification to mitigate the drawbacks of solvent extraction.

2. EXPERIMENTAL SECTION

2.1. Materials and Reagents

All chemicals were obtained from commercial sources and used as received unless otherwise specified. Poly(vinylbenzyl chloride) (PVBC) was purchased from Scientific Polymer Products (M_W 500,000 g/mol). Allyl-modified poly(arylene ether sulfone) (APAES, number-average molecular weight, $\bar{M}_n \sim$ 100,000 g/mol) was synthesized according to previously published methods.[31−33] For the synthesis of APAES, the following reagents were used: 2,2′-diallylbisphenol A (DABA, 85%), bisphenol A (BPA, ≥99%), bis(4-fluorophenyl)sulfone (DFDPS, 99%), *N*,*N*-dimethylacetamide (DMAc, 99.5%), chloroform ($CHCl_3$, 99%), diatomaceous earth (Celite 545), and potassium carbonate (K_2CO_3, ≥99%) were purchased from Sigma-Aldrich and were used as received. Hydrochloric acid (HCl, 36.5−38%), methanol (MeOH, 99%), and tetrahydrofuran (THF, 99%) were purchased from VWR and used as received. Toluene (99.9%) and THF Optima were purchased from Fisher Scientific and used after being passed through an MBraun SPS-800 solvent purification system.

Organic solvents used throughout the remaining procedures were tetrahydrofuran (THF) (unstabilized, HPLC grade, OmniSolve, Millipore Sigma), dimethylformamide (DMF, certified ACS, Fisher), and methanol (MeOH, certified ACS, Fisher). Lithium chloride was used in electrospinning (LiCl, 99+%, Acros Organics). PVBC membranes were cross-linked using potassium carbonate (99.8%, Fisher Scientific), potassium iodide (>99%, MP Biomedicals, LLC), and 2-(dimethylamino)ethylamine (Chem-Impex International). Deionized (DI) water (10 MΩ) was obtained through a RiOS 3 water purification system (Millipore Sigma, Burlington, Massachusetts). Inhibitors were removed from allyl methacrylate (AMA, Scientific Polymer Products) using hydroquinone/methyl ether (MEHQ) remover chromatographic packing (Scientific Polymer Products). AGET-ATRP used AMA, ascorbic acid (98+%, Acros Organics), 1,1,4,7,7-pentamethyldiethylenetriamine (PMDETA, 98+%, Acros Organics), copper(II) chloride ($CuCl_2$, ultradry, ≥99.995% metal basis, Alfa Aesar), and industrial grade nitrogen (size 300 Cylinder, CGA-580, Airgas Great Lakes Inc.).

Membranes were functionalized with cysteine (98+%, Alfa Aesar), FAM-thiol dye (DiagnoCine LLC), or Lanmodulin-based peptide (LanM1, sequence: CGGGDPDKDGTIDLKE, 95.0%+, GenScript Biotech), or scrambled Lanmodulin peptide (scramLanM1, sequence CGGGKGEDDDKTLDIP, 95.0%+, GenScript Biotech). The peptide sequences were designed as previously published[17] and selected for the present work given the relevant surface data found in that publication. Peptides were used for click reactions as received.

The initiators for the click reaction were lithium phenyl-2,4,6-trimethylbenzoylphosphinate (LiPTP, Sigma-Aldrich) or 2,2-dimethoxy-2-phenylacetophenone (DMPA, >98.0%, Tokyo Chemical Industries, Co.). Adsorption data were collected using solutions prepared from lanthanum nitrate hexahydrate (99.999%, Sigma-Aldrich), cerium nitrate hexahydrate (99.99%, Sigma-Aldrich), praseodymium nitrate hexahydrate (99.9%, Thermo Scientific), and neodymium nitrate hexahydrate (99.9%, Sigma-Aldrich). Analytical ion standards (NIST traceable, ISO certified 1000 ppm stock solutions) of lanthanum, cerium, praseodymium, and neodymium (in 2 wt % nitric acid) and phosphate (from potassium dihydrogen phosphate in H_2O) were purchased from High Purity Standards. Solutions of sodium hydroxide (1 N, Fisher) or nitric acid (Optima grade, Fisher) were diluted with deionized water (10 MΩ) and used for pH adjustments and dilutions.

2.2. PVBC−PAMA Membrane Synthesis: Electrospun Fibers with a 3D Network of Pendant Allyl Moieties

2.2.1. Electrospinning PVBC and Cross-Linking for Chemical Stability. PVBC membranes were fabricated by electrospinning according to a previously published procedure.[34] The composition of the polymer dope was 15 wt % PVBC and 0.5 wt % LiCl in THF. The PVBC membrane was electrospun onto Fisherbrand P4 filter paper which was taped to an aluminum foil-wrapped collector plate. All

https://doi.org/10.1021/acsaenm.4c00510
ACS Appl. Eng. Mater. 2024, 2, 2442−2453

membranes were electrospun for 10 min using a solution flow rate of 7 mL/h, ambient temperature, 50% relative humidity, spinneret-to-collector distance of 7 cm, and a voltage of 20 kV. After spinning, electrospun membranes were left out in a fume hood for 24 h to dry.

After drying, membranes were cut using a 40 mm die cutter (MAYHEW PRO 66006). The average mass was 0.17 g, which includes the electrospun fibers and the filter paper support. All cross-linking and AGET-ATRP reactions were performed with the support filter paper present. Each membrane was cross-linked using 0.36 g of K_2CO_3, 0.22 g of KI, and 109 μL of *N*,*N*-dimethylethylene diamine (DMEDA) in 25 mL of DI water. The concentrations of reactants in each jar were 104 mM of K_2CO_3, 53 mM of KI, and 40 mM of DMEDA. The cross-linking reaction proceeded for 2 days while mixing on a shaker table (LAB-LINE 3528−5 Orbit Environ-Shaker table) at room temperature. After drying, membranes were pressed for 10 min under 1 ton pressure using a pneumatic press (Carver Model C 12 Ton Manual Laboratory Press 3851) between two aluminum foil-coated plates (15 cm × 15 cm × 2.5 cm) to prevent loose fibers during further reactions.

2.2.2. Grafting Poly(allyl methacrylate) from the Cross-Linked PVBC Membrane Using AGET-ATRP. Before AGET-ATRP, the polymerization inhibitor, MEHQ, was removed from the AMA monomer using an inhibitor remover column. The column was prepared by packing a cotton ball into the bottom of a glass pipet. Then, the pipet was filled with 0.93 g of hydroquinone/methyl ether remover to create a column height of 7.2 cm. Liquid AMA was loaded onto the column and purified by gravity. By not applying pressure, the packed bed is not at risk of cracking, separation, or burping during purification. Four grams of inhibitor-free AMA were collected in a glass vial and stored temporarily in the refrigerator until use.

AGET-ATRP was conducted in glass jars with threaded caps containing a septum lid. To set up the reaction, 25 mL of DI water, measured using a graduated cylinder, ∼0.2 g of dried cross-linked PVBC membrane, and 4 g of inhibitor-free AMA were added to the jar. The jars were capped and placed on a shaker table to mix at a speed of 125 rpm, while the catalyst solution was prepared.

The catalyst solution was prepared by mixing 0.156 g of $CuCl_2$, 100 mL of DI water, and 108.4 μL of PMDETA in a glass jar. This volume of solution was enough to functionalize four membranes in separate glass jars—each with concentrations of 5.8 mM $CuCl_2$ and 0.45 mM PMDETA. Separately, a 30 mL solution of 0.25 M ascorbic acid solution in DI water was prepared in an amber jar. Once mixed, the ascorbic acid solution was stored for up to 2 weeks. To initiate AGET-ATRP, 25 mL of the catalyst solution was transferred into each sample jar using a calibrated pipet. Each jar was purged for 10 min with nitrogen using a multiport gas manifold (CR Brew Beer gas manifold−splitter with 5/16 in. barb fittings). After purging, a 0.5 mL transfer syringe with a permanently attached needle was used to add 464 μL of the AscA solution to each sample jar through the septum lid. The jars were placed on the shaker table at ambient temperature for 30 min to 24 h. The reaction was quenched by opening the jars and exposing the solution to oxygen.

After the reaction was quenched, each membrane was transferred to a jar containing 30 mL of a 50/50 (v/v%) DI water−methanol solution and mixed on the shaker table for 24 h to remove unreacted monomer or physically adsorbed polymer. Following the 24 h wash, each membrane was transferred to a jar containing 20 mL of a fresh 50/50 DI water−methanol solution and sonicated for 30 min. The grafted membranes were then dried in a vacuum oven for 24 h at room temperature and approximately 26 h in an Hg vacuum.

2.3. APAES Membrane Fabrication: Electrospun Membrane with Allyl Moieties in the Polymer Backbone

2.3.1. Electrospinning APAES Membranes with Allyl Backbones. An alternative membrane architecture with a single monolayer of adsorption sites was prepared using a specialized poly(arylene ether sulfone) polymer that contained pendant allyl groups (APAES) on 50% of the repeating units (Figure 1B,D). For clarification, "monolayer" in this article refers to a layer of adsorption sites that has a maximum thickness of a single peptide molecule covering the support fibers throughout the thickness of the fibrous membrane. The polymer was synthesized via a polycondensation reaction as previously published,[31−33] with a 1:1 stoichiometry between the dihalide (DFDPS) and bisphenol (BPA + DABA) monomers and the concentration of allyl groups (50%) was set by the BPA/DABA molar ratio of 1:1. The pendant allyl groups allowed click reactions to be performed directly on the polymer fibers as opposed to on a network of grafted polymer brush-like structures as in the PVBC−PAMA membranes.

APAES membranes were fabricated by electrospinning at room temperature. Pellets of the polymer were first dried under vacuum (26 in Hg vacuum) at 60 °C degrees overnight. The polymer dope solution contained 15 wt % APAES and 0.5 wt % LiCl in DMF. Electrospinning of APAES was performed in a home-built apparatus[34] using a solution flow rate of 1.0 mL/h, spinneret-to-collector distance of 7 cm, and a voltage of 30 kV. The ambient relative humidity was 31−32%. Fiber mats used for adsorption experiments were electrospun for 5 min each onto Fisherbrand P4 filter paper taped to a grounded plate wrapped in aluminum foil. Fiber mats used for porosity measurements were electrospun for 10−15 min directly onto the aluminum foil that covered the ground plate. All fiber mats were dried in a fume hood for at least 24 h. Membranes with a diameter of 30 mm were cut by using a die cutter. Membranes used for porosity measurements were scraped off the aluminum foil with a razor blade, while membranes used for adsorption were left on the filter paper backing. Then membranes were pressed using a pneumatic laboratory press between two aluminum foil-coated plates. The pressure was increased to 1 t for 10 min.

2.4. Membrane Functionalization: Thiol−Ene Click Reaction

Thiol−ene click reactions were used to install LanM1, cysteine, or thiol dye on the PVBC−PAMA membranes and/or APAES membranes. Due to the differences in polymer chemistry, the two membrane designs were functionalized using different conditions, as described below.

2.4.1. Aqueous Thiol−Ene Click Reactions for Cross-Linked PVBC−PAMA Membranes. PVBC−PAMA membranes with a diameter of 0.71 cm were cut from the dried grafted samples (post-AGET-ATRP) for use in click reactions. Each membrane (1.5 mg, filter paper no longer attached) was added to a 20 mL glass vial with 9 mg (0.005 mmol) of LanM1 peptide, 1.243 mg (0.004 mmol) of LiPTP photoinitiator, and 6 mL of DI water. The concentrations of reactants in the vial were 0.9 mM LanM1 and 0.7 mM LiPTP. The vials were capped using rubber stoppers and purged with N_2 for 10 min. The reaction proceeded on a shaker table at 230 rpm for 30 min −24 h under a 365 nm UV light (Analytik Jena, 15 W). The distance between the UV lamp and the membrane was approximately 3 cm. The temperature was left ambient and not controlled during the irradiation. Then, the functionalized membranes were washed with DI water overnight on a shaker table at 125 rpm to remove any physically adsorbed molecules. After the overnight wash, the membranes were sonicated for 30 min in fresh DI water and vacuum-dried at room temperature and approximately 26 h in Hg vacuum for 1 day. The same reaction conditions and molar concentrations were used to conduct thiol−ene click reactions with cysteine and the FAM-thiol dye.

2.4.2. Methanolic Thiol−Ene Click Reactions for APAES Membranes. APAES membranes with a diameter of 30 mm were cut using a die cutter and left on the filter paper backing for the duration of the click reaction procedure (∼72.5 ± 1.5 mg each, including filter paper backing). Prior to dissolving reagents, methanol was sparged with nitrogen gas for ∼1 h to decrease dissolved oxygen but was not kept air-free during reagent preparation. A typical solution was prepared by dissolving 50 mg (0.03 mmol) of LanM1 peptide and 2.3 mg (0.009 mmol) of DMPA initiator in 12 mL of sparged MeOH. A 3.0 mL portion of this solution, which had a final concentration of 2.5 mM peptide and 0.75 mM DMPA, was used for each membrane. The reaction setup is depicted in detail in the Supporting Information (SI) (Figure S1). In brief, an upside-down glass jar was used as the

https://doi.org/10.1021/acsaenm.4c00510
ACS Appl. Eng. Mater. 2024, 2, 2442−2453

reaction vessel to enable UV light to irradiate the solution and activate the initiator from above. To achieve this for the methanolic reactions, a threaded septum lid for a 60 mL wide-mouth jar was used as a base to hold the reaction solution in a small, elevated Petri dish. The Petri dish was elevated by a plastic mesh drain catcher, and the pieces were assembled using plastic tape. A 30 mm membrane coupon was placed in a Petri dish and covered with the reaction solution. The Petri dish platform with membrane and reagents as it now was attached to the septum lid, was covered by the 60 mL wide-mouth jar, and sealed. Then the atmosphere of the upside-down jar was purged with N_2 gas through the septum lid for 10−15 min. The methanol reaction solution did not leak out. Jars were placed under 365 nm UV light and agitated on a shaker table at 100 rpm for 2 h. The distance between the UV lamp and the Petri dish was 3 cm. Temperature was left ambient and not controlled during the irradiation. After the click reaction, membranes were rinsed 3 times with 2−3 mL of MeOH using a disposable plastic pipet, then submerged in fresh MeOH (∼20 mL each) overnight on the shaker table at 100 rpm. Then membranes were rinsed 3 times with ∼2−3 mL deionized H_2O and sonicated in fresh H_2O (∼20 mL each) for 30 min. After sonicating, membranes were rinsed once more with 2−3 mL of H_2O, and excess water was blotted off on weigh paper. Membranes were air-dried for 2−4 h in the fume hood and dried under approximately 26 in. Hg vacuum overnight at room temperature.

Slight modifications were made to the conditions to conduct thiol−ene click reactions of APAES membranes with L-cysteine. A 30 mm membrane coupon was divided into four quarters, each quarter-membrane placed in its own glass jar reactor and covered with 3.5 mL of a reaction solution containing 2.9 mM cysteine and 2.7 mM DMPA. The UV reaction conditions were the same as those for the methanol peptide functionalization, as described above.

2.5. Membrane Characterization: Chemistry and Morphology

2.5.1. Attenuated Total Reflectance Fourier-Transform Infrared Spectroscopy. Attenuated total reflectance Fourier-transform infrared spectroscopy (ATR-FTIR) was used to characterize the growth of poly(allyl methacrylate) (PAMA) from the cross-linked PVBC membrane fibers. Measurements were performed using a Nicolet iS50 FTIR instrument (Thermo Scientific) with a diamond crystal. Each measurement was collected as 32 scans with a resolution of 8 cm^{-1}. Background subtractions and spectra normalization were performed with Omnic 9 software, version 9.8.372.

2.5.2. Raman Spectroscopy. Raman spectroscopy was performed using a Renishaw inVia Raman microscope and a Leica DM 2500 M with a Renishaw CCD camera detector. Raman spectroscopy was used to qualitatively confirm the presence of the C═C group from the pendant allyl group of the PAMA chains before proceeding with the thiol−ene click reaction. Spectra were collected using a 785 nm edge laser (Innovative Photonic Solutions) at 10 or 100 mW and a 20× objective lens. Measurements were collected for 2 acquisitions with an exposure time of 10 s. Spectra were collected in 3 separate areas on the same membrane to assess the consistency of the membrane.

2.5.3. X-ray Photoelectron Spectroscopy. X-ray photoelectron spectroscopy (XPS) spectra were collected by using a PHI 5000 Versaprobe XPS instrument with a monochromatized Al Kα source. Approximately 0.1−0.5 mg of the membrane was mounted on a 1 in. holder with carbon tape (5 mm W × 20 mL, Ted Pella). Total pressure in the vacuum chamber was in the range of 1×10^{-6} to 1×10^{-7} Pa. Spectra were collected before and after thiol−ene click reaction to evaluate atom percent increases of sulfide. A measurement of cysteine powder was collected as a control to confirm an S peak shift after covalent bond formation. Survey spectra were collected between 0 and 1100 eV at a pass energy of 93.90 eV and an energy step of 0.4 eV. High-resolution spectra were collected with a pass energy of 23.5 eV and energy step 0.1 eV. Charge neutralization was used. Spectra were referenced to adventitious C (284.8 eV) using MultiPak software version 9.8.0.19. Atomic concentrations (%) were evaluated by integrating peak areas in the MultiPak software's Atomic Concentrations function, which accounts for the sensitivity factors supplied by the manufacturer.

2.5.4. Confocal Microscopy. To visualize the reactivity of the PAMA-grafted membrane, a fluorescent dye with thiol functionality (FAM-thiol) was reacted with a PAMA-grafted membrane. The reaction followed the same procedures as the peptide click reaction, except the dye was used in place of LanM1 at the same molar concentration. Once the membrane was dry, it was mounted on a glass slide and covered with a glass coverslip (Corning No. 11/2). The corners of the coverslip were sealed by using clear nail polish. The membrane was characterized using a Leica HyVolution SP8 confocal microscope with a 40× oil objective and 1.3 numerical aperture. An argon laser with an excitation wavelength of 488 nm was used as the light source. LAS X software version 3.5.5.19976 was used for analysis. The multifocus tool was used to obtain one composite image rendered from one *Z*-stack containing 7 images collected at 10 μm intervals.

2.5.5. Scanning Electron Microscopy. Membrane morphology was observed using an FEI/ThermoFisher Apreo 2S scanning electron microscope (SEM) with an Everhart−Thornley detector. Membranes were prepared for imaging by mounting them on an SEM pin stub (Standard SEM Pin Stub Mount, 12.7 mm outer diameter, 8 mm pin height, Ted Pella) with carbon tape (5 mm width, Ted Pella). Then, samples were sputter-coated with Pd by using a DentonVacuum DESK V Sputter Coater for 45 s. Samples were imaged with a working distance of 10 mm, a current of 13 or 50 pA, an accelerating electron voltage of 5.00 kV and a 0° tilt. The magnification of samples ranged from 500× to 10,000×. For measurement of both PVBC−PAMA and APAES membrane fiber diameters, measurements ($n_{PVBC-PAMA}$ = 7, n_{APAES} = 12) were made on a single pressed pristine membrane (postelectrospinning APAES and post-cross-linking PVBC) using the Apreo 2S software. The fiber diameter is reported as the mean ± one standard deviation.

2.5.6. Nuclear Magnetic Resonance Spectroscopy. One dimensional ^{1}H nuclear magnetic resonance (NMR) and diffusion-ordered spectroscopy (DOSY) was performed using a Bruker-BioSpin Avance III HD 500 MHz NMR spectrometer equipped with a Prodigy ultrahigh sensitivity Multinuclear Broadband CryoProbe. Samples of APAES polymers were dissolved in $CDCl_3$ to assess the alkene content and the success of early test reactions of the dissolved polymer with L-cysteine. DOSY measurement was performed with a stimulated echo experiment using bipolar gradients and longitudinal eddy current delay with the duration of rectangular gradient pulses, δ, of 4.7 ms and a delay between gradient pulses, Δ, of 140 ms, at a constant temperature, 298 K. Sixteen spectra were collected with gradient strength varied from 0.96 to 47.19 G/cm. Spectra were processed in MestreNova 14.3.1−31739. Samples of electrospun membranes that were reacted heterogeneously with L-cysteine were insoluble in common NMR solvents ($CDCl_3$ or d_6-DMSO) and could not be characterized by solution-state NMR spectroscopy. Therefore, characterization by XPS was favored.

2.5.7. Porosity Measurement of APAES Membranes. The porosity of PVBC−PAMA-LanM1 membranes was measured to be 83.7%, which fell within the range measured according to a prior publication.[34] APAES membranes were cut using either a 30 mm die cutter or cut to a size with similar weight (3.9 ± 1.0 mg), scraped from the foil backing, and then pressed using a pneumatic laboratory press as described above. Membranes were soaked in isopropanol, a nonswelling solvent, on a shaker table at 50−75 rpm for 25 h. The porosity was calculated by eq 1.

$$\varepsilon = \frac{(m_w - m_d)/\rho_i}{(m_w - m_d)/\rho_i + (m_d)/\rho_p} \quad (1)$$

where m_w and m_d are the mass (g) of the wet and dry membranes, respectively, and ρ_i and ρ_p are the density of isopropanol and the polymer (g/cm^3), respectively. The density of the polymer was estimated at 1.24 g/cm^3, and the density of polysulfone (average M_w ∼ 35,000) at 25 °C was listed by Sigma-Aldrich (Product 428302).

https://doi.org/10.1021/acsaenm.4c00510
ACS Appl. Eng. Mater. 2024, 2, 2442−2453

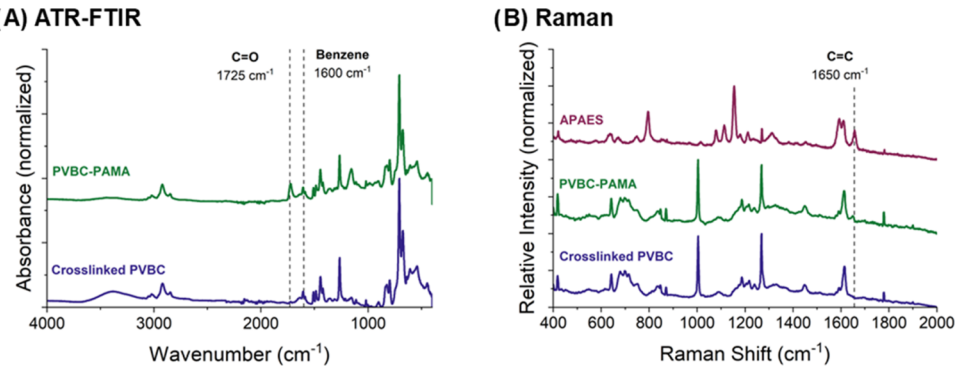

Figure 2. (A) ATR-FTIR spectra for cross-linked PVBC and PAMA-grafted membranes and (B) Raman spectra for cross-linked PVBC, PAMA-grafted, and APAES membranes. For both membrane designs, the pendant allyl group is present on the membrane surface prior to the thiol−ene click reaction.

Three membranes were tested and the error is represented as the standard deviation.

2.6. Membrane Performance: Equilibrium Adsorption

2.6.1. Adsorption Experiments. Equilibrium adsorption experiments were performed with lanthanum, cerium, praseodymium, and neodymium to assess the ability of the peptide-functionalized membranes to adsorb lanthanide ions. These ions were chosen for this study as they are the lanthanides with the highest concentrations in our target phosphogypsum feedstock.[5] Single-species adsorption experiments were performed with each lanthanide using an initial concentration of 104−109 μM (15 ppm) at pH 4.2 and 5.2. A follow-up experiment is described in the SI, which exposed the APAES membranes loaded with La and Ce from the pH 5.2 batch of experiments to 103 μM (10 ppm) phosphate solution (pH 5.85).

For pH 4.2 lanthanide adsorption experiments, 104−108 μM (15 ppm) solutions were prepared by diluting a commercial stock solution (1000 ppm lanthanide in 2 wt % nitric acid) using a calibrated micropipette. The pH of each solution was adjusted to 4.2 ± 0.2 by using solutions of NaOH (1 M) and HNO_3 (0.3 M). Adsorption experiments were performed by placing 1 mg of a peptide-functionalized membrane (without filter paper backing) into a 2 mL microcentrifuge tube with 1.5 mL of 104−108 μM (15 ppm) lanthanide ion solution. The microcentrifuge tube was equilibrated at room temperature for 24 h on a rotisserie tube rotator at 40 rpm. Following equilibration, the solution was filtered using a 13 mm, 0.22 μm PVDF syringe filter (VWR) to remove membrane particulates prior to analyzing the metal concentrations in solution by inductively coupled plasma optical emission spectroscopy (ICP-OES).

For pH 5.2 adsorption experiments, a 3.5−3.6 mM (500 ppm) stock solution of each lanthanide (La, Ce, Pr, Nd) was prepared from the appropriate lanthanide nitrate hydrate in DI H_2O in a volumetric flask and diluted to 104−109 μM (15 ppm) using a calibrated micropipette. The pH of this solution was found to be 5.2 ± 0.2, without adjustment of pH. The adsorption experiments followed the same protocols as the pH 4.2 experiment, except the pH 5.2 experiment used a volume of 1.25 mL.

Initial and equilibrium ion concentrations were quantified using ICP-OES. Calibration standards were prepared with concentrations of 0.07−700 μM (0.01−100 ppm) in 2 wt % HNO_3. Samples were prepared for ICP-OES analysis by diluting 1 mL of the filtered sample with HNO_3 to achieve a final concentration of 2 wt % nitric and a volume of 10 mL. The emission wavelength scanned for each lanthanide are as follows: 333.749 nm (La), 407.570 (Ce), 422.532 (Pr), 410.945 (Nd).

The equilibrium binding capacity of the membrane, Q_e, was calculated after measuring the equilibrium concentration according to eq 2.

$$Q_e = \frac{(C_0 - C_e) \times V}{m} \quad (2)$$

Where C_0 is the initial ion concentration, C_e is the equilibrium ion concentration, V is the solution volume (L), and m is the membrane mass (g). At least three replicates using different membranes were performed for each pH and lanthanide.

2.6.2. Statistical Analysis. Statistical analysis was conducted using Minitab ($\alpha = 0.05$). Normality and equal variance were assumed in all statistical tests based on acceptable ranges of variance, normality plots, and residual plots (full statistical analysis results found at the end of the Supporting Information document). Analysis of variance (ANOVA) followed by Tukey's *post hoc* testing was performed on equilibrium adsorption data to compare the amount of each REE bound to each membrane. A two-sample, one-tailed t test was performed on adsorption data for La on each membrane to test whether the amount of ion bound to the membrane functionalized with regular LanM1 was higher than the amount bound to the membrane functionalized with scrambled LanM1.

Analysis of variance (ANOVA) followed by Tukey's *post hoc* testing was also performed on time optimization experiments shown in Figure S2.

For phosphate experiments described in SI section 8, two-sample, one-tailed t tests were used to test whether the adsorption of phosphate to lanthanide-loaded (La and Ce) LanM1 peptide APAES membranes was higher than the amount adsorbed to the respective control membranes that had no peptide treatment.

3. RESULTS AND DISCUSSION

3.1. Membrane Characterization

3.1.1. Spectroscopic Characterization of the AGET-ATRP Reaction for PVBC−PAMA and Electrospun APAES. Characteristic peaks identified in the ATR-FTIR spectra support the conclusion that PAMA was grafted from the PVBC−PAMA membranes. ATR-FTIR spectra are shown in Figure 2A for cross-linked PVBC and PAMA-grafted membranes. Absorbance at 1735 cm^{-1} is attributed to the C═O of the PAMA. That peak is compared to absorbance at 1600 cm^{-1} which is ascribed to the unchanging benzene ring of the PVBC. The ratio of these peak intensities was used to assess AGET-ATRP time optimization experiments (Figure S2). Time had a significant impact on the peak ratio, and the 2 h reaction time was chosen as there is no significant increase in grafted polymer at longer reaction times.

The pendant allyl moieties must be present in both PVBC−PAMA membranes and APAES membranes to perform the thiol−ene click reaction. Allyl functional groups have a characteristic Raman shift peak at 1650 cm^{-1}. The growth of this peak between cross-linked and PAMA-grafted membranes, and its presence following electrospinning of APAES membranes, supported the preservation of the allyl moieties.

https://doi.org/10.1021/acsaenm.4c00510
ACS Appl. Eng. Mater. 2024, 2, 2442−2453

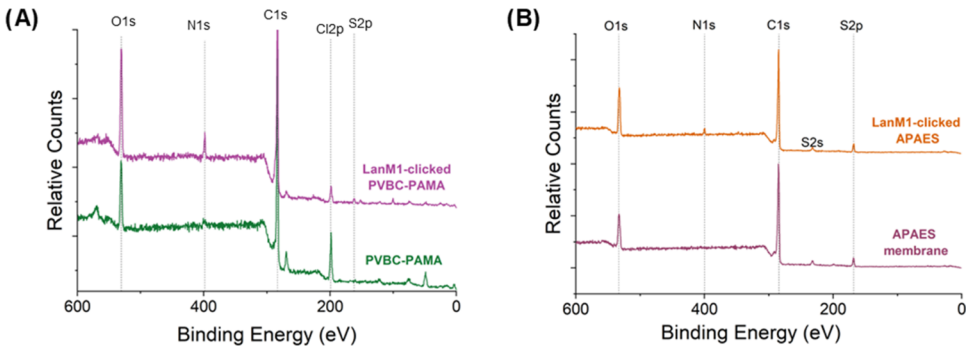

Figure 3. X-ray photoelectron spectra of membranes before and after peptide functionalization. The intensity of N 1s and O 1s signals was observed to increase in both membrane types with peptide addition. (A) Cross-linked PVBC−PAMA-grafted and LanM1-clicked PVBC−PAMA. In addition to N 1s and O 1s, a new S 2p sulfide signal was observed from peptide addition. (B) APAES and LanM1-clicked APAES. The observed S 2p signal arises from sulfone in the polymer backbone. Sulfide signals from the peptide were too weak to be characterized in LanM1-clicked APAES membranes, but an increase in the intensity of the O 1s and a new N 1s signal was observed.

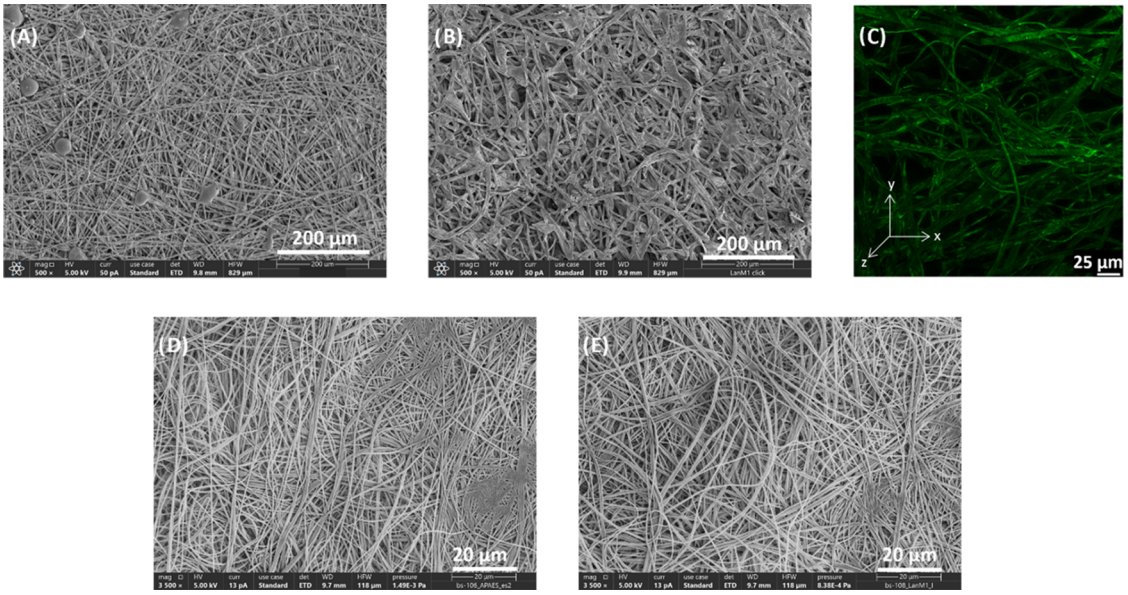

Figure 4. SEM images at 500× for (A) PVBC−PAMA membrane, (B) LanM1-clicked PVBC−PAMA membrane, and (C) confocal microscopy composite image of FAM-thiol dye-clicked PVBC−PAMA membrane and at 3500× for the (D) APAES membrane, and (E) LanM1-clicked APAES membrane.

Both spectra are shown in Figure 2B. NMR spectroscopy of electrospun APAES was also used to characterize the allyl functionality (Figure S3).

3.2. Thiol−Ene Click Reaction

At this stage, both PVBC−PAMA membranes and APAES membranes were ready for thiol−ene click reactions.

3.2.1. Characterization of Membranes After Thiol−Ene Click Reactions. As an initial test, a reaction of solubilized APAES polymer with L-cysteine in DMF was performed to confirm that a covalent bond formed between the polymer and a thiol-containing amino acid. The reaction product was characterized by DOSY NMR (Figure S4) spectroscopy, which indicated a broad signal attributed to cysteine protons with roughly the same diffusion coefficient as the bulk polymer. Fifty percent of the initial allyl groups were converted during the reaction in DMF based on analysis of ^{1}H NMR spectroscopy (Figure S4). Historically, 100% conversion has been observed for click reaction of the allyl groups in APAES polymers,[31−33] but incomplete conversion under these conditions is likely affected by poor solubility of L-cysteine in DMF. For solid membranes, click reactions were performed with a solution of thiol-containing reagent (peptide, dye, or small molecule) under UV light. The success of the solid phase click reaction was characterized by XPS or confocal microscopy.

Initially, the aqueous condition used for the PVBC−PAMA membranes was attempted for the APAES membranes. However, a higher surface ratio of cysteine to polymer was observed by XPS when using methanol as a solvent for that membrane (Figure S5); therefore, the methanolic click conditions were used for all subsequent APAES membrane preparation. Equal cysteine functionalization was observed for both the aqueous and the methanolic click conditions on the PVBC−PAMA membranes. The aqueous click condition was used for all subsequent PVBC−PAMA membrane preparation.

The indicator of a successful thiol−ene click reaction in XPS is a clear peak shift at 162 eV corresponding to the formation of a sulfide (S−C) bond (Figure S6). Figure 3 shows spectra collected using XPS for both PVBC−PAMA-grafted membranes and APAES membranes before and after the LanM1

https://doi.org/10.1021/acsaenm.4c00510
ACS Appl. Eng. Mater. 2024, 2, 2442−2453

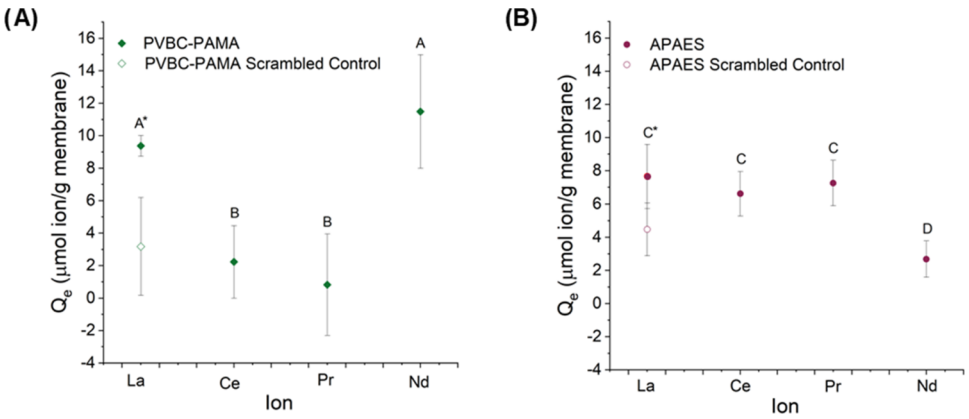

Figure 5. Equilibrium adsorption results for both (A) PVBC−PAMA and (B) APAES membranes. Data are represented as the mean ± standard deviation with $n = 3$. Q_e is the binding capacity as defined by eq 2. Significant differences in equilibrium adsorption among lanthanides for each membrane were determined by performing ANOVA and Tukey's *post hoc* test assuming equal variances. Groups A and B resulted from the PVBC−PAMA test, Groups C and D resulted from the separate APAES test and are not comparable with Groups A and B. Groups that do not share a letter within each graph are statistically different ($p < 0.05$) at the 95% confidence interval. Significant differences for La adsorption to LanM1 membranes versus scrambled control membranes for each membrane type were determined by performing a two-sample, one-tailed *t* test assuming equal variance. (*) represents *p*-value <0.05 compared to the control.

click. In PVBC−PAMA, the appearance of the sulfide peak at 162 eV for the LanM1-clicked sample along with the growth of the N and O peaks supports the attachment of the peptide. Time optimization results are shown in Figure S7. The 3 h reaction time was chosen for all subsequent PVBC−PAMA materials, as there is no notable increase in sulfide content for longer reaction times. A 2 h irradiation time was maintained for APAES as this was the duration typically used in previous click reactions with the APAES polymer.[31−33] In APAES membranes, the polymer backbone contains a sulfone moiety visible in the spectrum, but the sulfide signal that could be seen with cysteine is too weak to characterize in APAES-LanM1 materials. The polymer backbone contains no nitrogen, so the new N 1s signal is the result of peptide attachment, as is the increase in the O 1s signal.

Further analysis of XPS peak ratios is described in the SI (Figures S8 and S9 and Tables S1 and S2) to show reproducibility of click reactions. The peak ratio analysis supports the conclusion that the amount of peptide in membranes modified with scrambled LanM1 fell within the range of membranes modified with LanM1. Quantitative comparisons between membrane types risk misrepresentation due to differences in chemistry.

3.3. Membrane Morphology

SEM images show that the integrity of the polymer fibers was largely maintained following the click reaction under UV light for both types of membranes (PVBC−PAMA membranes, Figure 4A,B; APAES membranes, Figure 4D,E). Some broken fibers were observed for both membrane types, and some deformation of the APAES fibers was observed from pressing the membranes (1 t, 10 min) to prevent loosening of the fiber mat. SEM images throughout earlier steps of the preparation of PVBC−PAMA membranes can be found in the SI (Figures S10−S12).

The porosity of the APAES mats was measured at 92 ± 5%. Measurements of the diameter of the APAES fibers in SEM images showed thinner fibers (0.525 ± 0.158 μm) than PAMA-grafted, cross-linked, PVBC membrane fibers (3.007 ± 0.685 μm diameter). An analysis by Boi et al. investigated the relationship between fiber diameter, porosity, and surface area for nonwoven fibers.[35] Applying this analysis, the APAES membrane (0.525 μm diameter, ∼90% porosity) would have a surface area per volume of fiber of 0.8 m^2/mL. Likewise, the PAMA-grafted, cross-linked, PVBC membrane (3.007 μm ± 0.685 μm diameter, ∼80% porosity) would have a surface area of roughly 0.3 m^2/mL. These measurements indicate that APAES membranes have approximately 2.5× higher surface area than the PVBC−PAMA membranes prior to LanM1 functionalization.

Confocal microscopy imaging supports the success of the thiol−ene click reaction of the PVBC−PAMA membrane with the FAM-thiol dye, Figure 4C. Importantly, individual images taken at 10 μm increments through the thickness of the membrane, Figure S13, provide direct visual evidence of functionalization throughout the depth of the membrane, approximately 60 μm. This data marks an improvement over the previous design that was limited to the top surface of the membrane (approximately 3 μm).[30] Functionalizing through the depth of the membrane has the potential to increase the membrane capacity on a per-mass basis.

3.4. Equilibrium Adsorption

Single-species equilibrium adsorption experiments were used to quantify each lanthanide bound to the membranes after exposure to 104−109 μM (15 ppm) lanthanide solutions. These concentrations were chosen to compare directly to prior work.[21] Results from both PVBC−PAMA and APAES membranes for pH 5.2 are shown in Figure 5 and a similar plot for adsorption results at pH 4.2 is shown in Figure S14. Adsorption is pH sensitive, as shown by lower binding at pH 4.2. Based on prior work comparing EF-hand peptide-functionalized membranes with a scrambled control membrane,[30] the sequence of amino acids in the binding region of the peptide is not anticipated to impact peptide loading of the materials. This hypothesis is supported in this work by analysis of the XPS peak ratios found in Table S2.

Several observations can be made from the data. First, both PVBC−PAMA and APAES membranes were capable of adsorbing at least one REE in single-species adsorption experiments. This is an exciting step that demonstrates the feasibility of peptide-modified membrane materials for

https://doi.org/10.1021/acsaenm.4c00510
ACS Appl. Eng. Mater. 2024, 2, 2442−2453

Table 1. Lanthanide-Binding Biosorbent Equilibrium Capacities in Single Concentration Adsorption Experiments (La and Nd)

ligand, *support*	adsorption experiment conditions[a,b,c] (mass adsorbent, volume solution, pH)	La, equilibrium capacity (μmol ion/g sorbent)	Nd, equilibrium capacity (μmol ion/g sorbent)	analysis technique[f]	refs
L-lysine (brush-like), poly(ether sulfone)-*graft*-poly(glycidyl methacrylate) *membranes*	15 mg membrane, 15 mL solution, pH 5.25	33 ± 12	18 ± 2	UV−vis assay	21
LanM1, PVBC−PAMA (brush-like) *membranes*	1 mg membrane, 1.25 mL solution, pH 5.2	9.4 ± 0.6	11 ± 3.5	ICP-OES	this work
LanM1, APAES, (monolayer) *membranes*	1 mg membrane; 1.25 mL solution, pH 5.2	7.7 ± 1.9	2.7 ± 0.8	ICP-OES	this work
LanM1 on gold *nanoparticles*	∼10.6 mg nanoparticles; 1.5 mL, pH 5−5.5[d]		4.10[d]	UV−vis assay	17
lanmodulin protein, dendrimeric magnetic *nanoparticles*	2.5 mg nanoparticles, 1 mL solution, pH 5 MES buffer[e]	6.3[e]	5.7[e]	ICP-MS	16

[a]Equilibrated at least 24 h unless specified. [b]Concentration of lanthanide 100−110 μM, unless specified. [c]pH of unbuffered solutions was adjusted by the addition of minimal amounts of HCl, HNO_3, or NaOH. [d]90 μM REE initial concentration. [e]Samples equilibrated for 60 min in 70 μM REE concentration. [f]ICP-MS = Inductively coupled plasma mass spectrometry. UV−vis assay = ultraviolet−visible spectrophotometric assay by arsenazo-III complexation with lanthanide.

lanthanide adsorption. Focusing on lanthanum, both LanM1-clicked membranes adsorbed statistically more lanthanum than scrambled controls. This result indicates that, when installed on the polymer fibers, the specific sequence of the LanM1 peptide has a direct positive effect on lanthanide adsorption that cannot be attributed simply to electrostatic interactions of the peptides' charged groups with the ions.

When considering La, PVBC−PAMA adsorbed ∼9 μmol/g of membrane and APAES adsorbed ∼8 μmol/g of membrane from a pH 5.2 solution with a C_0 of 108 μM. Despite differences in the membrane designs, the LanM1 membranes had similar equilibrium capacities at the tested conditions. Initially, this result was surprising because the PVBC−PAMA membranes were designed to contain LanM1-decorated brush-like structures and anticipated to have a higher capacity than the monolayer-functionalized APAES fibers. To rationalize this, we considered the morphology of the two membranes. The APAES membrane had thinner fiber diameters (0.525 ± 0.158 μm) than the PVBC−PAMA membrane (3.007 ± 0.685 μm), resulting in roughly 2.5x higher surface area than PVBC−PAMA (analysis described in Section 3.3). However, the addition of the AMA polymer network by AGET-ATRP is expected to increase the effective areal density of allyl sites. The ability for brush-like structures to increase capacity was previously demonstrated using weak anion exchange membranes with amine functional brushes grafted from regenerated cellulose membranes. The polymer grafted membranes had 3× greater capacity for protein binding than commercial monolayer-functionalized membranes.[36] Based on the difference in fiber surface area, it is plausible that the PAMA brush-like network compensates for the lower surface area, achieving a capacity that is on the same order of magnitude as the monolayer on the thinner fibers. An additional consideration is that PAMA is a hydrophobic polymer (contact angle of 79°)[37] and the thiol−ene click reaction was performed in water. If the PAMA brush-like structures have limited swelling in water, the pendant allyl moieties may not be fully accessible for the peptide attachment. While brush conformation on fibers is challenging to confirm directly,[38] others have shown that incorporating hydrophilic comonomers increases lysosome binding capacity.[39] Related to the hydrophobicity, steric hindrance may be a challenge in the PAMA-grafted membrane as the areal brush density,[40] spacers within the brushes,[41] and flexibility of the chain[42] have been shown to impact ligand loading and binding capacity. If the accessibility of the PAMA brush-like structures is hindered due to steric hindrance or limited swelling, the peptides could attach to the accessible PAMA surface in a way that more closely mimics a monolayer on the fibers. Future work will explore more hydrophilic chemistries than PAMA and study their impact on adsorption.

For each membrane type, ANOVA statistical analysis revealed that the type of ion significantly impacted equilibrium capacity and was followed by Tukey's *post hoc* test. Points that share a letter (A, B and C, D) in Figure 5 are statistically similar. For the APAES membrane, the adsorption of La, Ce, and Pr was not found to be statistically different, while the adsorption of Nd was statistically lower than that of the other lanthanides. For PVBC−PAMA, the adsorption of La and Nd was not found to be statistically different, and the adsorption of Ce and Pr was less than both La and Nd. Previously, the lanthanide affinity of LanM1 bound to a gold surface was estimated using quartz-crystal microbalance with dissipation, which found higher affinity for Ce than for Nd based on the equilibrium adsorption constants.[17] Based on the single test condition in this work, the APAES membranes are consistent with the gold-bound LanM1; however, a more rigorous analysis of the materials will be necessary by constructing an equilibrium adsorption isotherm to clarify trends in selectivity.

Table 1 places our new biosorbent materials in context with other lanthanide-binding biosorbents in the literature. Since full isotherm data are not available for all materials, including those in the present work, data are tabulated for discussion for adsorbents at a single C_0 concentration. Lanthanum and neodymium were common adsorbates reported for most materials and serve as the basis of the discussion. Cerium and praseodymium data are additionally listed in Table S3. For all membranes, the initial concentrations were 100−110 μM depending on the lanthanide. For the gold nanoparticles, the initial concentrations were 90−100 μM, and for magnetic nanoparticles, the initial concentrations were 70 μM.[16] The pH in all adsorption experiments reported in Table 1 was 5−5.5.

Based on the available data, La adsorption can be used to discuss the impact of ligand size on adsorption capacity. The three ligands include the lanmodulin protein, LanM1 peptide, and L-lysine—ranging from largest to smallest. The peptide-functionalized LanM1-APAES and LanM1−PVBC-PAMA membranes adsorbed a comparable quantity of lanthanide (same order of magnitude) as the protein functionalized

https://doi.org/10.1021/acsaenm.4c00510
ACS Appl. Eng. Mater. 2024, 2, 2442−2453

nanoparticles,[16] while L-lysine-functionalized membranes adsorbed more lanthanum at the tested conditions.[21] The lanmodulin protein magnetic nanoparticles effectively enhanced the material surface area by using a dendritic network extending from the nanoparticle, which may account for the protein being on the same order of magnitude as the smaller peptide. Although the L-lysine membranes had higher capacity, a disadvantage of small molecule ligands is that they are expected to exhibit less specific metal binding and may be susceptible to competition at high concentrations of di- or monovalent metals compared to a biological ligand with a coordination environment suited for lanthanides. The observation of higher adsorption for the small L-lysine ligand encourages the hypothesis that the size of the ligand plays a role in capacity and suggests that further optimization of peptide is worth considering, as both high specificity and capacity are pursued.

The role of the support structure has already been discussed above in the context of fiber surface area of LanM1 peptide-functionalized APAES and PVBC−PAMA membranes, but these data can also be contextualized with respect to LanM1 gold nanoparticles (i.e., a solid support). Using data for neodymium adsorption, we found that LanM1 membranes and LanM1 gold nanoparticles adsorbed similar quantities of lanthanide (same order of magnitude). Given that the equilibrium capacity of these specific materials is similar on the laboratory-scale, practical factors and scale-up analysis may play a deciding role in future industrial adoption.

With respect to the broader appeal of these materials, there has been significant recent interest in lanthanide-containing materials for the purpose of capturing excess agricultural phosphate.[43,44] To test the viability of this future application for our membranes, we did a brief follow-up study of lanthanide-loaded peptide membranes for phosphate capture. Results from phosphate equilibrium adsorption experiments with the La- and Ce-containing APAES membranes are shown and discussed in the SI (Figure S15). The experiment supported that lanthanide-containing membranes are worthy of further exploration for phosphate recovery and remediation projects.

4. CONCLUSIONS

In summary, our study characterized the chemistry and morphology of two new peptide-functionalized materials and performed adsorption experiments using adjacent REEs. Cross-linked, PVBC membrane fibers with grafted PAMA brush-like structures and APAES membrane fibers were functionalized with lanmodulin-derived peptides using a UV-initiated, thiol−ene click reaction. To confirm that polymer brush-like structures were grafted from PVBC fibers, ATR-FTIR measurements were performed. Raman spectroscopy was used to confirm that the allyl groups in both membrane scaffolds were preserved before proceeding with the thiol−ene click reaction. Functionalized membranes were characterized via SEM and XPS, which showed that fiber morphology was preserved throughout functionalization and supported the covalent addition of the peptide. Depth of functionalization was qualitatively characterized using a representative small molecule, FAM-thiol dye, and showed functionalization throughout the membrane depth (~60 μm).

Equilibrium adsorption studies were conducted at a single ion concentration (15 ppm) and pH 5.2 for La, Ce, Pr, and Nd. Adsorption results showed that the lanmodulin peptide sequence maintains its ability to bind when it is immobilized on a solid membrane surface. Capacity of both of these new materials is on the same order of magnitude, which is surprising as the brush-like morphology was expected to have a higher capacity than the monolayer. This could be a result of the fiber diameter, as the monolayer material has a much lower fiber diameter (0.525 μm vs 3.007 μm), resulting in a 2.5× higher overall surface area. The grafted hydrophobic brush-like structures on the PVBC−PAMA material may also be impacting the material's capacity, which will be explored in future work. Promisingly, the membranes showed statistically different equilibrium capacities for some ions, but further material testing must be performed to determine whether the selectivity between ions is influenced.

This contribution is an exciting step toward using bioinspired membrane adsorbers for REE recovery from low-concentration waste sources. Future work will continue to modify the PVBC−PAMA design to increase hydrophilicity and evaluate the affinity and selectivity for immobilized lanmodulin peptides on a three-dimensional (3D) brush-like network.

■ ASSOCIATED CONTENT

Supporting Information

The Supporting Information is available free of charge at https://pubs.acs.org/doi/10.1021/acsaenm.4c00510.

Reaction setup for methanol reactions, AGET-ATRP time optimization, NMR data and analysis, XPS data and analysis, SEM images, pH 4.2 lanthanide adsorption data, biosorbents in single concentration adsorption experiments (La, Ce, Pr, and Nd), phosphate binding experiment, and tables of statistical output (PDF)

■ AUTHOR INFORMATION

Corresponding Authors

Julie N. Renner − *Department of Chemical and Biomolecular Engineering, Case Western Reserve University, Cleveland, Ohio 44106, United States;* orcid.org/0000-0002-6140-4346; Phone: 216-368-2905; Email: julie.renner@case.edu

Christine E. Duval − *Department of Chemical and Biomolecular Engineering, Case Western Reserve University, Cleveland, Ohio 44106, United States;* orcid.org/0000-0002-8630-5483; Phone: 216-368-8613; Email: Christine.Duval@case.edu

Authors

Lianna Johnson − *Department of Chemical and Biomolecular Engineering, Case Western Reserve University, Cleveland, Ohio 44106, United States;* orcid.org/0000-0002-0396-8426

Bernadette L. Schneider − *Department of Chemical and Biomolecular Engineering, Case Western Reserve University, Cleveland, Ohio 44106, United States;* orcid.org/0000-0002-4383-7068

Husain Mithaiwala − *Department of Chemical Engineering, School for Engineering of Matter, Transport and Energy, Arizona State University, Tempe, Arizona 85287, United States*

Matthew D. Green − *Department of Chemical Engineering, School for Engineering of Matter, Transport and Energy,*

https://doi.org/10.1021/acsaenm.4c00510
ACS Appl. Eng. Mater. 2024, 2, 2442−2453

Arizona State University, Tempe, Arizona 85287, United States; orcid.org/0000-0001-5518-3412

Complete contact information is available at: https://pubs.acs.org/10.1021/acsaenm.4c00510

Author Contributions

§L.J. and B.L.S. contributed equally to this work. L.J. and B.L.S. were the primary authors responsible for writing this manuscript, conducting experiments, and analyzing data. L.J. performed all work related to PVBC−PAMA membranes. B.L.S. performed work related to APAES membranes. H.M. synthesized the APAES polymer. M.D.G. guided the development of the APAES polymer. J.N.R. and C.E.D. guided experiments, data analysis, and manuscript preparation. All authors contributed to the article and approved the submitted version.

Notes

The authors declare the following competing financial interest(s): MDG is co-founder of NuAria, LLC and owns 50% equity interest in the company. The work of this manuscript is not directly related to the activities of the company.

■ ACKNOWLEDGMENTS

This work was supported by the National Science Foundation (Award Nos. 2133549 and 1836719), the United States Department of Agriculture (Award No. 2018−68011−28691), and the Global Center for Water Treatment (part of the State of Arizona's Water Innovation Initiative). The authors acknowledge the following facilities at Case Western Reserve University: Chemical Engineering Instrumentation Core Facility for use of the Renishaw inVia Raman microscope and Thermo Scientific Nicolet iS50 Fourier-transform infrared spectrometer; the Swagelok Center for Surface Analysis of Materials for use of the PHI 5000 Versaprobe X-ray photoelectron spectrometer and FEI/ThermoFisher Apreo 2S scanning electron microscope; the Northeast Ohio High Field Nuclear Magnetic Resonance Facility for use of the Bruker-BioSpin Avance III HD 500 MHz NMR spectrometer; and the School of Medicine Light Microscopy Core Facility which was funded by NIH Grant S10-OD024996.

■ REFERENCES

(1) Xie, F.; Zhang, T. A.; Dreisinger, D.; Doyle, F. A Critical Review on Solvent Extraction of Rare Earths from Aqueous Solutions. *Miner. Eng.* **2014**, *56*, 10−28.

(2) Smith, Y. R.; Kumar, P.; McLennan, J. D. On the Extraction of Rare Earth Elements from Geothermal Brines. *Resources* **2017**, *6* (3), No. 39.

(3) Mukaba, J.-L.; Eze, C. P.; Pereao, O.; Petrik, L. F. Rare Earths' Recovery from Phosphogypsum: An Overview on Direct and Indirect Leaching Techniques. *Minerals* **2021**, *11* (10), No. 1051.

(4) Yang, X.; Salvador, D.; Makkonen, H. T.; Pakkanen, L. Phosphogypsum Processing for Rare Earths Recovery—A Review. *Nat. Resour.* **2019**, *10* (9), 325−336.

(5) Liang, H.; Zhang, P.; Jin, Z.; DePaoli, D. Rare Earths Recovery and Gypsum Upgrade from Florida Phosphogypsum. *Miner. Metall. Process.* **2017**, *34* (4), 201−206.

(6) Zhang, P. Comprehensive Recovery and Sustainable Development of Phosphate Resources. *Procedia Eng.* **2014**, *83*, 37−51.

(7) *Mineral Commodity Summaries*; US Geological Survey, 2024.

(8) Salehi, H.; Maroufi, S.; Mofarah, S. S.; Nekouei, R. K.; Sahajwalla, V. Recovery of Rare Earth Metals from Ni-MH Batteries: A Comprehensive Review. *Renewable Sustainable Energy Rev.* **2023**, *178*, No. 113248.

(9) Ambaye, T. G.; Vaccari, M.; Castro, F. D.; Prasad, S.; Rtimi, S. Emerging Technologies for the Recovery of Rare Earth Elements (REEs) from the End-of-Life Electronic Wastes: A Review on Progress, Challenges, and Perspectives. *Environ. Sci. Pollut. Res.* **2020**, *27* (29), 36052−36074.

(10) Horwitz, E. P.; McAlister, D. R.; Bond, A. H.; Barrans, R. E., Jr Novel Extraction of Chromatographic Resins Based on Tetraalkyldiglycolamides: Characterization and Potential Applications. *Solvent Extr. Ion Exch.* **2005**, *23* (3), 319−344.

(11) Ye, Q.; Wang, D.; Wei, N. Engineering Biomaterials for the Recovery of Rare Earth Elements. *Trends Biotechnol.* **2024**, *42*, No. 575.

(12) Brown, R. M.; Mirkouei, A.; Reed, D.; Thompson, V. Current Nature-Based Biological Practices for Rare Earth Elements Extraction and Recovery: Bioleaching and Biosorption. *Renewable Sustainable Energy Rev.* **2023**, *173*, No. 113099.

(13) Dong, Z.; Mattocks, J. A.; Deblonde, G. J.-P.; Hu, D.; Jiao, Y.; Cotruvo, J. A., Jr.; Park, D. M. Bridging Hydrometallurgy and Biochemistry: A Protein-Based Process for Recovery and Separation of Rare Earth Elements. *ACS Cent. Sci.* **2021**, *7* (11), 1798−1808.

(14) Mattocks, J. A.; Jung, J. J.; Lin, C.-Y.; Dong, Z.; Yennawar, N. H.; Featherston, E. R.; Kang-Yun, C. S.; Hamilton, T. A.; Park, D. M.; Boal, A. K.; Cotruvo, J. A. Enhanced Rare-Earth Separation with a Metal-Sensitive Lanmodulin Dimer. *Nature* **2023**, *618* (7963), 87−93.

(15) Sree, H.; Swarup, G.; Gupta, S.; Pushpavanam, K. Gravity-Driven Separation for Enrichment of Rare Earth Elements Using Lanthanide Binding Peptide-Immobilized Resin *ACS Appl. Bio Mater.* 2024, DOI: 10.1021/acsabm.3c01280.

(16) Ye, Q.; Jin, X.; Zhu, B.; Gao, H.; Wei, N. Lanmodulin-Functionalized Magnetic Nanoparticles as a Highly Selective Biosorbent for Recovery of Rare Earth Elements. *Environ. Sci. Technol.* **2023**, *57* (10), 4276−4285.

(17) Verma, G.; Hostert, J.; Summerville, A. A.; Robang, A. S.; Garcia Carcamo, R.; Paravastu, A. K.; Getman, R. B.; Duval, C. E.; Renner, J. Investigation of Rare Earth Element Binding to a Surface-Bound Affinity Peptide Derived from EF-Hand Loop I of Lanmodulin. *ACS Appl. Mater. Interfaces* **2024**, *16* (13), 16912−16926.

(18) Freitag, R.; Splitt, H.; Reif, O.-W. Controlled Mixed-Mode Interaction Chromatography on Membrane Adsorbers. *J. Chromatogr. A* **1996**, *728* (1), 129−137.

(19) Ghosh, R. Protein Separation Using Membrane Chromatography: Opportunities and Challenges. *J. Chromatogr. A* **2002**, *952* (1), 13−27.

(20) Chitpong, N.; Husson, S. M. High-Capacity, Nanofiber-Based Ion-Exchange Membranes for the Selective Recovery of Heavy Metals from Impaired Waters. *Sep. Purif. Technol.* **2017**, *179*, 94−103.

(21) Yu, M.; Renner, J. N.; Duval, C. E. A Lysine-Modified Polyethersulfone (PES) Membrane for the Recovery of Lanthanides. *Front. Chem.* **2020**, *8*, No. 512.

(22) Park, D. M.; Reed, D. W.; Yung, M. C.; Eslamimanesh, A.; Lencka, M. M.; Anderko, A.; Fujita, Y.; Riman, R. E.; Navrotsky, A.; Jiao, Y. Bioadsorption of Rare Earth Elements through Cell Surface Display of Lanthanide Binding Tags. *Environ. Sci. Technol.* **2016**, *50* (5), 2735−2742.

(23) Park, D. M.; Brewer, A.; Reed, D. W.; Lammers, L. N.; Jiao, Y. Recovery of Rare Earth Elements from Low-Grade Feedstock Leachates Using Engineered Bacteria. *Environ. Sci. Technol.* **2017**, *51* (22), 13471−13480.

(24) Cotruvo, J. A.; Featherston, E. R.; Mattocks, J. A.; Ho, J. V.; Laremore, T. N. Lanmodulin: A Highly Selective Lanthanide-Binding Protein from a Lanthanide-Utilizing Bacterium. *J. Am. Chem. Soc.* **2018**, *140* (44), 15056−15061.

(25) Cook, E. C.; Featherston, E. R.; Showalter, S. A.; Cotruvo, J. A., Jr. Structural Basis for Rare Earth Element Recognition by

Methylobacterium Extorquens Lanmodulin. *Biochemistry* **2019**, *58* (2), 120−125.
(26) Deblonde, G. J.-P.; Mattocks, J. A.; Park, D. M.; Reed, D. W.; Cotruvo, J. A., Jr.; Jiao, Y. Selective and Efficient Biomacromolecular Extraction of Rare-Earth Elements Using Lanmodulin. *Inorg. Chem.* **2020**, *59* (17), 11855−11867.
(27) Hussain, Z.; Kim, S.; Cho, J.; Sim, G.; Park, Y.; Kwon, I. Repeated Recovery of Rare Earth Elements Using a Highly Selective and Thermo-Responsive Genetically Encoded Polypeptide. *Adv. Funct. Mater.* **2022**, *32* (13), No. 2109158.
(28) Gutenthaler, S. M.; Tsushima, S.; Steudtner, R.; Gailer, M.; Hoffmann-Röder, A.; Drobot, B.; Daumann, L. J. Lanmodulin Peptides − Unravelling the Binding of the EF-Hand Loop Sequences Stripped from the Structural Corset. *Inorg. Chem. Front.* **2022**, *9* (16), 4009−4021.
(29) Xu, M.; Su, Z.; Renner, J. N. Characterization of Cerium (III) Ion Binding to Surface-Immobilized EF-Hand Loop I of Calmodulin. *Pept. Sci.* **2019**, *111* (6), No. e24133.
(30) Hostert, J. D.; Sepesy, M. R.; Duval, C. E.; Renner, J. N. Clickable Polymer Scaffolds Enable Ce Recovery with Peptide Ligands. *Soft Matter* **2023**, *19* (15), 2823−2831.
(31) Yang, Y.; Behbahani, H. S.; Morgan, B. F.; Beyer, F. L.; Hocken, A.; Green, M. D. Synthesis and Thermomechanical Characteristics of Zwitterionic Poly(Arylene Ether Sulfone) Copolymers. *Polymer* **2023**, *264*, No. 125522.
(32) Yang, Y.; Ramos, T. L.; Heo, J.; Green, M. D. Zwitterionic Poly(Arylene Ether Sulfone) Copolymer/Poly(Arylene Ether Sulfone) Blends for Fouling-Resistant Desalination Membranes. *J. Membr. Sci.* **2018**, *561*, 69−78.
(33) Shokrollahzadeh Behbahani, H.; Mithaiwala, H.; Marques, H. L.; Wang, W.; Freeman, B. D.; Green, M. D. Quaternary Ammonium-Functionalized Poly(Arylene Ether Sulfone) Random Copolymers for Direct Air Capture. *Macromolecules* **2023**, *56* (16), 6470−6481.
(34) Sepesy, M.; Banik, T.; Scott, J.; Venturina, L. A. F.; Johnson, A.; Schneider, B. L.; Sibley, M. M.; Duval, C. E. Chemically Stable Styrenic Electrospun Membranes with Tailorable Surface Chemistry. *Membranes* **2023**, *13* (11), No. 870.
(35) Lavoie, J.; Fan, J.; Pourdeyhimi, B.; Boi, C.; Carbonell, R. G. Advances in High-Throughput, High-Capacity Nonwoven Membranes for Chromatography in Downstream Processing: A Review. *Biotechnol. Bioeng.* **2024**, *121*, 2300−2317.
(36) Bhut, B. V.; Wickramasinghe, S. R.; Husson, S. M. Preparation of High-Capacity, Weak Anion-Exchange Membranes for Protein Separations Using Surface-Initiated Atom Transfer Radical Polymerization. *J. Membr. Sci.* **2008**, *325* (1), 176−183.
(37) Voccia, S.; Claes, M.; Jérôme, R.; Jérôme, C. Sequential Electrografting and Ring-Opening Metathesis Polymerization: A Strategy for the Tailoring of Conductive Surfaces. *Macromol. Rapid Commun.* **2005**, *26* (10), 779−783.
(38) Choi, B.-C.; Choi, S.; Leckband, D. E. Poly(N-Isopropyl Acrylamide) Brush Topography: Dependence on Grafting Conditions and Temperature. *Langmuir* **2013**, *29* (19), 5841−5850.
(39) Himstedt, H. H.; Qian, X.; Weaver, J. R.; Wickramasinghe, S. R. Responsive Membranes for Hydrophobic Interaction Chromatography. *J. Membr. Sci.* **2013**, *447*, 335−344.
(40) Bao, Z.; Bruening, M. L.; Baker, G. L. Control of the Density of Polymer Brushes Prepared by Surface-Initiated Atom Transfer Radical Polymerization. *Macromolecules* **2006**, *39* (16), 5251−5258.
(41) Islam, T.; Naik, A. D.; Hashimoto, Y.; Menegatti, S.; Carbonell, R. G. Optimization of Sequence, Display, and Mode of Operation of IgG-Binding Peptide Ligands to Develop Robust, High-Capacity Affinity Adsorbents That Afford High IgG Product Quality. *Int. J. Mol. Sci.* **2019**, *20* (1), No. 161.
(42) Chambre, L.; Maouati, H.; Oz, Y.; Sanyal, R.; Sanyal, A. Thiol-Reactive Clickable Cryogels: Importance of Macroporosity and Linkers on Biomolecular Immobilization. *Bioconjugate Chem.* **2020**, *31* (9), 2116−2124.
(43) He, Q.; Zhao, H.; Teng, Z.; Wang, Y.; Li, M.; Hoffmann, M. R. Phosphate Removal and Recovery by Lanthanum-Based Adsorbents: A Review for Current Advances. *Chemosphere* **2022**, *303*, No. 134987.
(44) Zhang, X.; Mai, Y.; Xian, X.; Hu, L.; Huang, J.; Yuan, H.; Lin, X. Adsorption and Removal of Phosphate from Wastewater Using Lignin-Based Adsorbent Modified with Lanthanide: Characterization, Performance, and Mechanisms. *Ind. Eng. Chem. Res.* **2022**, *61* (49), 18069−18079.

https://doi.org/10.1021/acsaenm.4c00510
ACS Appl. Eng. Mater. 2024, 2, 2442−2453